ACS OMEGA

http://pubs.acs.org/journal/acsodf

Article

Coupling Mechanism of Dissipated Energy−Infrared Radiation Energy of the Deformation and Fracture of Composite Coal-Rock under Load

Xin Li, Hao Li,* Zhen Yang,* Hui Zuo, Weiman Sun, Hongzhu Li, and Yan Li

Cite This: *ACS Omega* 2022, 7, 8060−8076

Read Online

ACCESS | Metrics & More | Article Recommendations

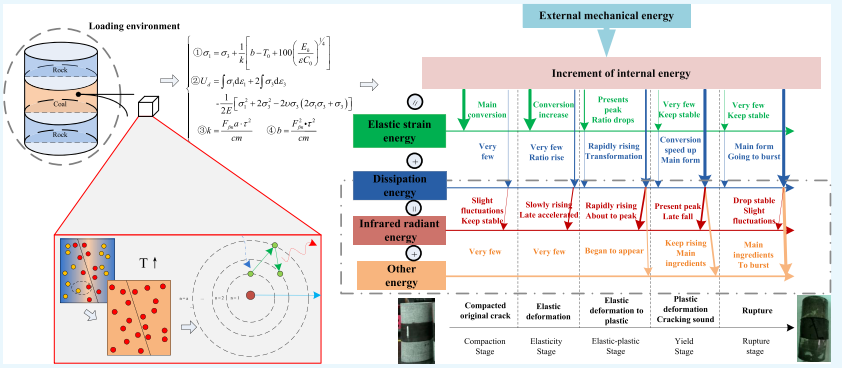

ABSTRACT: The fracture of composite coal-rock under load is the process of energy conversion. As the dissipative energy composition, there is a correlation between the infrared radiation energy and the coal-rock states. Based on theories of theoretical mechanics, modern quantum mechanics, thermodynamics, and other disciplines, first, this paper explained the causes of infrared radiation energy in the process of coal-rock fracture by using the microanalysis method. After that, the mathematical model of dissipation energy−infrared radiation energy coupling was deduced and established, and the experimental analysis was carried out under different loading conditions. The analysis shows that the conversion of mechanical energy and internal energy in the process of loading caused constant collisions between molecules in coal-rock, which led to a temperature rise. After entering the excited state, molecules have to transition to a lower energy level, which generates infrared radiation. The experimental results show that there was a strong correlation between energy characteristic parameters, which is consistent with the established relationship. In addition, the energy conversion and dissipated energy changes in the loading process had stages. Before the elastic−plastic stage, the dissipated energy obtained by coal-rock energy conversion was less, but it increased rapidly in the later stage, which eventually led to the fracture of coal-rock. In the early elastic−plastic period, infrared radiation energy was the main component of the dissipated energy and its variation trend was consistent with the dissipated energy. After that, the infrared radiation energy remained stable, but the dissipation energy still increased. At this time, infrared radiant energy was no longer the main component of dissipated energy. And the infrared radiation energy dropped rapidly before coal-rock fracture, which had certain precursory characteristics. The coupling mechanism of dissipated energy−infrared radiation energy can be used to explain the failure reason of composite coal-rock under different loading conditions from the perspective of energy, which will provide a new idea for assisting the prediction of coal-rock dynamic disasters.

1. INTRODUCTION

With the deep mining of coal seam, the problems of coal-rock dynamic disaster prevention and control such as rockburst have been paid more attention.[1−5] In this context, researchers have studied various problems arising in the process of rockburst, for example, the internal or external causes of rockburst,[6,7] the risk assessment of rockburst accident,[8−10] the law of coal-rock cracking,[11] the law of impact signal transmission,[12] etc. In these research fields, coal-rock dynamic disaster prediction plays an important role, which is directly related to the safety of life and property. As a result, many researchers hope to find a method of disaster prediction by studying the characteristics of coal-rock in the process of fracture.

Received: December 26, 2021
Accepted: February 11, 2022
Published: February 22, 2022

https://doi.org/10.1021/acsomega.1c07289
ACS Omega 2022, 7, 8060−8076

At present, most of the existing research results in this field are merely on the variation law or coupling relationship of observable physical parameters: Li X. *et al.*[13−15] used numerical simulation to study the coupling mechanism of the temperature, stress, and electromagnetic field of composite coal-rock in the process of loading; verified the simulation conclusion based on experiments; and established the multi-physical field coupling model of composite coal and rock and the triaxial failure criterion under different unloading conditions. Liu X. *et al.*[16] studied the variation law of electromagnetic radiation in the process of uniaxial compression of coal-rock and established the relationship between the Hurst index and deformation, and the research results have a positive significance for rockburst prediction. Zheng K.H. *et al.*[17] modeled the failure process of coal-rock under a dynamic impact load based on the finite element and discrete element models of images. They considered that the spatial distribution and loading direction of samples had an impact on material strength and failure mode, and verified that XCT image modeling was an effective analysis method. Guo J.Y. *et al.*[18] studied the difference between acoustic emission and failure of coal-rock based on a uniaxial compression experiment, believed that acoustic emission characteristics could better describe the failure characteristics of coal-rock, and proposed a failure warning value of 100−150. Li L. *et al.*[19] studied the fracture evolution law of single fracture prefabricated fractures in Longmaxi shale using a CCD camera and acoustic emission monitoring equipment. The study showed that there was a strong correlation between the acoustic emission and rock fracture state, so this law could be used to judge the rock state. Although existing researches can reveal the failure law of coal-rock to a certain extent, there are still some limitations in the nature of coal-rock fracture and prediction of its fracture.

The fracture of coal-rock under load is a thermodynamic process, and its deformation state is related to internal and external energy transformation.[20−23] To master the relationship between the failure law of composite coal-energy transformation, researchers from various countries have made some achievements in recent years: Duan M.K. *et al.*[24] conducted an experimental analysis on the permeability characteristics, acoustic emission characteristics, and energy dissipation of coal-rock during cyclic loading, and the results showed that the dissipated energy increases with the loading process in a quadratic function relationship and is positively correlated with the deformation trend. Li X.L. *et al.*[25] established the elastic−plastic brittle rockburst model of coal-rock and introduced the concept of volume energy potential function to effectively analyze the characteristics of microseismic and electromagnetic radiation. Xue Y. *et al.*[26] carried out theoretical analysis and FLAC simulation on the mechanism of coal pillar rockburst and classified the rockburst risk by using energy density characteristics. The study found that elastic strain energy would release suddenly when rockburst disaster occurred. Mohammadali S. *et al.*[27] studied the elastic strain energy of rock, combined the energy and accumulation degree, and analyzed the two methods by numerical simulation, which can effectively predict the rockburst trend. Yang L. *et al.*[28] conducted uniaxial compression and cyclic loading and unloading tests on two-layer coal-rock mass, studied the evolution law of each energy in the process of loading, and preliminarily discussed the energy driving mechanism of failure of coal-rock mass. Li B.B. *et al.*[29] studied the damage of coal-rock under mechanical−thermal coupling based on triaxial compression experiments at different temperatures and found that energy evolution had stage characteristics and that dissipated energy was the main cause of damage. Through experiments or theoretical analysis by some researchers, it can be known that the dissipated energy is closely related to the fracture state of coal-rock, and it is feasible to predict coal-rock's deformation trend from the perspective of energy. As a general term for many energies, dissipative energy is very difficult to obtain directly. To solve this problem, most researchers calculate the elastic strain energy and total energy to indirectly obtain the dissipated energy and the energy state of coal-rock. This method has certain theoretical significance, but it is difficult in engineering applications. The reason is that the calculation of elastic strain energy must rely on the mechanical parameters, so it is inevitable to use a large number of contact sensors, which does not meet the application requirements of the engineering field. To sum up, it is of great significance to find a method of obtaining the dissipative energy state without contact, which will help to further establish the relationship between energy and coal-rock's state and finally realize the application of the energy theory in reality.

Infrared radiation energy is a kind of energy that can be obtained by a noncontact method, and it is closely related to the internal state of the measured object. As a result, infrared radiation analysis technology has been widely used in various fields requiring noncontact measurement, for example, vital signs monitoring,[30,31] power equipment damage monitoring,[32,33] celestial movement,[34] medical diagnosis assistance,[35] geological survey,[36] etc. In the loading process of coal-rock, infrared radiation energy is a part of dissipated energy, and there is a certain coupling between them. In view of this feature, some scholars have studied the variation of infrared radiation energy and its characteristic parameters in the process of coal-rock's fracture in recent years, and some achievements have been made: Xu L. *et al.*[37] experimentally studied the relationship between temperature and rock energy and also discussed the relationship between temperature and granite energy storage capacity (ESC), suggesting that the increase of temperature reduced the energy storage capacity of rock, thus promoting the occurrence of rockburst. Li Z.H. *et al.*[38] analyzed the variation trend of thermal infrared radiation temperature in the process of fracture and also defined the concepts of damage precursor point and critical precursor point. Liu X.X. *et al.*[39] studied the influence of humidity and water content in a humid environment on the average temperature of rock failure, believing that the more water content there is, the faster is the rock destroyed and the more likely it is to produce an acoustic emission phenomenon, and temperature can be used as a precursor judgment indicator. Chen G.Q. *et al.*[40] studied the thermal precursor information of true triaxial loading failure of rock and believed that the thermal infrared index should be introduced in the prediction of rock loading to enhance the accuracy of judgment. Liu C.Y. *et al.*[41] divided rockburst into four stages according to carrying capacity and analyzed the relationship between energy variation trend including thermal radiation temperature and sample failure. Huang F.R. *et al.*[42] explained the variation law of rock and IR under uniaxial compression and believed that there was a strong linear relationship between temperature and stress. Wang B.X. *et al.*[43] conducted experiments on samples under low-temperature conditions to study the influence of temperature on mechanical parameters and construct relevant numerical relationships. It is considered that the dissipated energy of rock increases linearly with loading and the temperature is related to the amount of energy

https://doi.org/10.1021/acsomega.1c07289
ACS Omega 2022, 7, 8060−8076

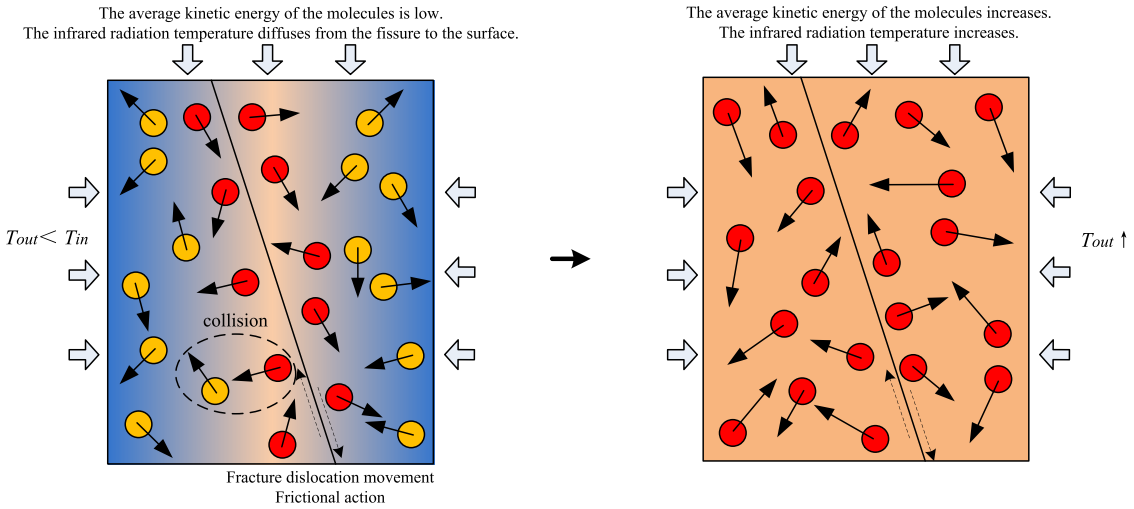

Figure 1. Changes of molecular motion in composite coal-rock during loading.

accumulation. Although there were some researches on infrared radiation or temperature associated with infrared radiation energy, most of them were the fitting and analysis of a single physical quantity. However, there are few researches on infrared radiation energy as a form of dissipative energy, let alone the relationship between them. Therefore, the research in this field is still in its infancy.

As an important internal cause of coal-rock fracture, the change of dissipated energy is difficult to measure without contact in the existing results. In addition, the existing prediction methods based on energy theory are difficult to apply in practice. However, as one of the components of dissipative energy, infrared radiation energy can be measured by a noncontact method, which provides a way to solve this problem. Based on these, in this paper, the coupling model of dissipated energy and infrared radiation energy of coal-rock under a loading condition was established by using thermodynamics, theoretical mechanics, and statistical theory. Meanwhile, the relationship between these energies was further verified and analyzed through experiments. On this basis, the relationship between energy change and the mechanical state of composite coal-rock during the loading process was established, and the law of energy transformation in coal-rock was deeply analyzed. This makes it possible to judge the stress state of coal-rock without contact and provides a new idea for preventing coal-rock dynamic disaster.

2. THEORY AND METHOD

2.1. Microphysical Mechanism Analysis of Coal-Rock under Loading. According to a large number of previous experiments and results, the external force continued to act on the coal-rock during the loading process, and the measured surface temperature and external infrared radiation intensity of samples would increase in this process. According to the first law of thermodynamics, under ideal adiabatic conditions, all mechanical energy generated by work done by force is converted into internal energy, which will cause the internal energy of the object to increase. On this basis and in refs 44 and 45, it can be seen that in the loading process of composite coal-rock, the increment of internal energy will eventually be expressed in the form of elastic strain energy and dissipated energy. The elastic strain energy is reflected by the elastic deformation of the object, and other energies that are not reflected by elastic deformation can be regarded as one of the components of the dissipated energy.[44,45] Although infrared radiation energy is related to the temperature of the object, it is essentially a kind of electromagnetic radiation energy. Therefore, infrared radiation and temperature are two completely different physical quantities. At the same time, infrared radiant energy can also be regarded as one of the components of dissipative energy. To sum up, the balance between mechanical energy generated by the work done by external forces and various energies is shown in eq 1.

$$W_m = W_i = W_e + W_d = W_e + (E_h + W_\Delta) \quad (1)$$

where W_m is mechanical energy of work done by an external force (J), W_i is the increased internal energy (J), W_e is the elastic strain energy transformed from mechanical energy (J), W_d is the dissipated energy converted from mechanical energy (J), E_h is the infrared radiation energy converted in the process (J), and W_Δ is the energy form of dissipated energy except infrared radiation energy (J).

Composite coal-rock is a kind of rock and soil material whose internal structure arrangement is loose, and there are some tiny cracks in the original state. These provide the physical basis for the energy transformation of coal-rock under load. From the microscopic point of view, the temperature rise of coal-rock is related to the molecular thermal movement. During loading, dislocation movement is easy to occur between the two contact surfaces of the original tiny crack inside so that the friction does work, which leads to local heating inside the sample and the overall internal energy enhancement. With the advance of coal-rock loading, the high-speed molecules moving disorderedly on the surface of the microcrack constantly collide with the low-speed molecules located deep in the interior, which allow low-speed molecules to get some or all of their kinetic energy from the high-speed ones. This can be regarded as the process in which the energy generated by the external work flows into the samples. The longer the loading time is, the more intense is the process, resulting in more frequent and disorderly molecular movements in coal-rock. In this process, the average kinetic energy of the internal whole increases, while the disorder and intensity of molecular motion are significantly enhanced. According to thermodynamic laws and experiments in ref 46, the average surface temperature of composite coal-rock continues to rise in this process.

Figure 1 shows the variation trend of molecular motion in coal-rock during loading, where the shade of color indicates the

https://doi.org/10.1021/acsomega.1c07289
ACS Omega 2022, 7, 8060−8076

temperature and the length of the arrow indicates how fast the molecules are moving. As can be seen from Figure 1, at the initial stage, most of the molecules in the composite coal-rock move at a low speed. At this time, coal-rock is in a steady state of energy balance. When an external force is applied to the coal-rock, the external force makes the original microcracks in coal-rock closely contact and increases the possibility of sliding friction movement between crack contact surfaces. This makes most of the external mechanical energy W_m convert into the kinetic energy of the molecules located on the surface of the fracture and further intensifies the molecular movement at the fracture. This process promotes the continuous transformation of external mechanical energy into internal energy of coal-rock and also causes the formation of multiple micro heat sources in the cracks of composite coal-rock. These heat sources increase the temperature in the cracks inside coal-rock and continuously release heat outward, finally increasing the temperature of the whole. Combined with the above analysis, under ideal adiabatic conditions, the coal-rock's increment of internal energy W_i is equal to external mechanical energy W_m. As can be seen in Figure 1, at the beginning, the color of cracks is orange and the color outside is blue, and then the orange part gradually spreads out, indicating heat transfer during loading. At this time, the surface temperature of coal-rock T_{out} is obviously lower than the internal temperature T_{in}. With loading advancing, the probability of high-speed molecules hitting low-speed molecules increases, which gradually increases the kinetic energy of the external molecules and intensifies the overall molecular thermal motion inside the coal-rock. Therefore, this also leads to an increase in the external surface temperature T_{out}. As can be also seen from Figure 1, because of constant heat transfer from the inside out, the surface temperature T_{out} gradually increases and the temperature of the sample gradually changes from low temperature blue to high temperature orange. This process completes the transformation of external mechanical energy into internal energy of coal-rock.

In the above content, the mechanism of temperature rise and the energy conversion process of coal-rock during loading were mainly discussed, but the reason for the infrared radiation change caused by loading was not explained. What follows is an analysis of why this happens based on quantum theory.

In the above process, the thermal motion of coal-rock internal microscopic particles is enhanced by energy conversion, thus forming some internal heat sources and releasing heat continuously. The temperature increase also causes the particles to be excited from the ground state to the excited state. To return to stability, particles must transition from high energy to low. According to Bohr's theory, internal particles emit a large number of photons as they transition, which is called electromagnetic radiation. And because these radiations are temperature-related, they are also called infrared radiation. This process is shown in Figure 2. In this process, part of the internal energy of the composite coal-rock W_i is transformed into infrared radiation energy E_h, which conforms to the description of eq 1.

2.2. The Theoretical Analysis of Coupling Relationship between Dissipated Energy and Infrared Radiation Energy. *2.2.1. The Analysis of Stress−Temperature Coupling Relationship.* To reveal the coupling relationship between various energies in the loading process of composite coal-rock, it is very important to analyze and characterize the parameters of energies. The rise of temperature is related to the change of internal energy. According to the first law of thermodynamics,

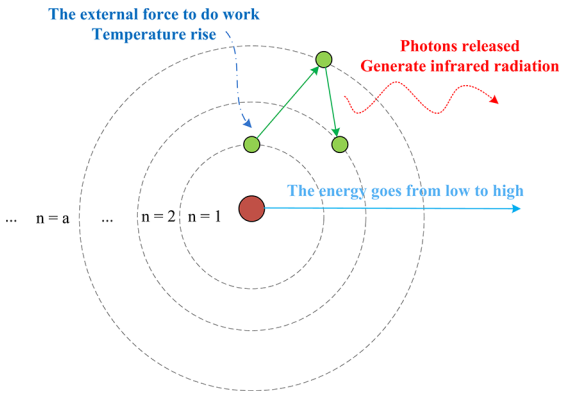

Figure 2. Microscopic mechanism of infrared radiation generation.

when work transformation is not considered, the increment of internal energy only comes from the absorption of energy, which is in the form of heat transfer. Therefore, it can be considered that when no work is done, the essence of rising temperature of objects is the transfer of heat between different objects.[47] Combined with previous analysis, infrared radiation is generated by the excitation of temperature. As a result, the change of infrared radiant energy is closely related to temperature; thus, temperature can be regarded as a characteristic parameter representing infrared radiant energy. It can be known from the literature that the dissipated energy is calculated according to the stress−strain curve, so stress can be considered as the characteristic parameter of it. To sum up, before studying the coupled relationship between dissipated energy and infrared radiant energy, the stress−temperature relationship of coal-rock should be clarified.

To facilitate the analysis of the relationship between stress and temperature, the composite coal-rock is divided into n unit volume microelements, and then the No.i element is selected for analysis, as shown in Figure 3.

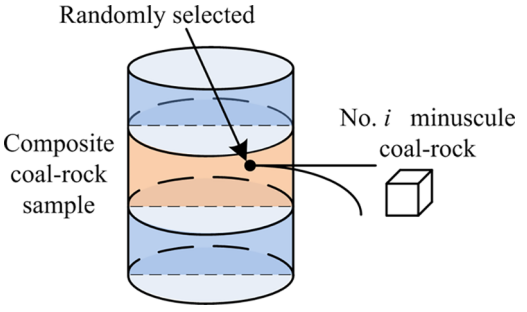

Figure 3. Composite coal-rock unit volume diagram.

According to ref 48 and the previous analysis, the temperature rise of each coal-rock's micro-unit is related to the change of internal energy, and the reasons for the change are as follows: (1) heat conduction of other elements and (2) the work of friction being converted to internal energy. Both processes increase the internal energy of each unit and thus increase the temperature. These physical processes both make the thermal motion of internal molecules more intense, which causes the internal energy of the No.i block of coal-rock per unit volume Q_i to increase over time. The process can be expressed as

$$Q_i = Q_f + Q_a \quad (2)$$

https://doi.org/10.1021/acsomega.1c07289
ACS Omega 2022, 7, 8060−8076

where Q_f is the increase in internal energy by converting work done by the external force (J) and Q_a is the increase in internal energy by heat conduction (J).

According to the heat conduction theory and relevant literature,[49,50] heat conduction leads to an increase in internal energy, which in turn leads to an increase in temperature. Combined with refs 51−53, when No.i per unit coal-rock's temperature rises $\Delta T_i K$ in unit time dt, the net internal energy obtained by heat conduction dQ_a is

$$dQ_a = \lambda\left(\frac{\partial^2 \Delta T_i}{\partial x^2} + \frac{\partial^2 \Delta T_i}{\partial y^2} + \frac{\partial^2 \Delta T_i}{\partial z^2}\right)dV\,dt \tag{3}$$

where λ is the thermal conductivity coefficient of coal-rock. At any time t, No.i coal-rock per unit volume dV obtains the net internal energy through heat conduction Q_a is

$$\begin{aligned} Q_a &= \lambda\left(\frac{\partial^2 \Delta T_i}{\partial x^2} + \frac{\partial^2 \Delta T_i}{\partial y^2} + \frac{\partial^2 \Delta T_i}{\partial z^2}\right)t\cdot dV \\ &= \lambda\nabla^2(\Delta T_i)t\cdot dV \end{aligned} \tag{4}$$

where ∇^2 is the Laplacian operator, which is $(\partial^2/\partial x^2 + \partial^2/\partial y^2 + \partial^2/\partial z^2)$.

Although there is adhesion between mineral particles in composite coal-rock, there are some original cracks, which can be regarded as the bud of cracks.[40] When the component of external resultant force in the direction of fracture development is greater than its maximum static friction force F_{fm} during loading, sliding friction will occur on both sides of the original fracture inside the composite coal-rock. Then the energy conversion from mechanical energy to internal energy is realized by the action of friction F_{fm}, and it is accompanied by the generation of heat, which makes the composite coal-rock local temperature rise. In addition, because of the different directions of the original cracks in coal-rock, these cracks' effective action time of sliding friction τ is not the same, but τ can be regarded as a constant only related to the sample structure. Under different loading conditions, the samples are subjected to different external forces: Under uniaxial loading, the combined stress σ_{all} at the original crack is the axial principal stress σ_1. The resultant stress σ_{all} under triaxial loading is deviator stress, and its value is the difference between axial stress and lateral stress $(\sigma_1 - \sigma_3)$. Sliding friction occurs only when the combined force component is greater than the maximum static friction force F_{fm}. According to the thermodynamic theorem and the calculation of equivalent velocity, at any time t, No.i per unit volume's internal energy Q_f of coal-rock increased by energy conversion though friction can be written as

$$\begin{aligned} Q_f &= \frac{\sigma_{all}F_{fm}\tau_i^2\cos\theta_i\cdot dS - F_{fm}^2\cdot\tau_i^2}{dm} \\ &= \frac{\sigma_{all}F_{fm}\tau_i^2\cos\theta_i\cdot dS - F_{fm}^2\cdot\tau_i^2}{\rho dV} \end{aligned} \tag{5}$$

where σ_{all} is the combined stress in the original fracture space of the No.i coal-rock unit (Pa), dS is unit area of friction surface (m^2), θ is angle between the resultant force and the direction of the original crack (°), τ_i is effective time of sliding friction action of internal cracks (s), and dm is the unit mass, whose value is 1 kg.

Assuming that the temperature of the No.i coal-rock unit rises $\Delta T_i K$ per unit time dt, its heat source intensity q_i is

$$q_i = \Delta T_i \rho c\,dx\,dy\,dz \tag{6}$$

where ρ is the density of coal-rock (kg/m^3), c is the specific heat capacity of coal-rock [J/(kg·K)], and dxdydz = dV is the unit volume (m^3).

Then, the internal energy increased by the unit volume of the No.i coal-rock Q_i at any time t is

$$\begin{aligned} Q_i &= \int_0^t q_i\,dt = \int_0^t \Delta T_i \rho c\,dx\,dy\,dz\,dt \\ &= \Delta T_i\cdot t\rho c\,dx\,dy\,dz \end{aligned} \tag{7}$$

So the temperature of No.i coal-rock unit T_i at any time t is

$$T_i = T_0 + \Delta T_i\cdot t = T_0 + \frac{Q_i}{\rho c dV} \tag{8}$$

where T_0 is the initial temperature of coal-rock (K).

By combining eqs 2, 4, and 5, it can be deduced that No.i coal-rock unit temperature T_i at any time t is

$$T_i = \frac{F_{fm}\tau_i^2\cos\theta_i}{\rho c dV}\sigma_{all} - \frac{F_{fm}^2\cdot\tau_i^2}{\rho^2 c dV^2} + \frac{\lambda\nabla^2(\Delta T_i)\cdot t}{\rho c} + T_0 \tag{9}$$

Equation 9 is a partial differential equation. $(\Delta T_i\cdot t)$ can be solved by writing boundary value conditions for coal-rock units, and the unitary function model of temperature T_i combined stress σ_{all} can be obtained. The model has some theoretical significance for analyzing the development of fracture from the microscopic point of view. According to eq 9, the average temperature T_{ave} of macroscopic composite coal-rock is

$$\begin{aligned} T_{ave} &= \frac{\sum_{i=1}^n T_i}{n} \\ &= \frac{1}{n}\sum_{i=1}^n\left(\frac{F_{fm}\tau_i^2\cos\theta_i}{\rho c dV}\cdot\sigma_{all} - \frac{F_{fm}^2\cdot\tau_i^2}{\rho^2 c dV^2}\right) + \frac{\lambda\cdot t}{n\rho c}\sum_{i=1}^n\nabla^2(\Delta T_i) + T_0 \\ &= \frac{F_{fm}\sum_{i=1}^n(\tau_i^2\cos\theta_i)}{n\rho c dV}\cdot\sigma_{all} - \frac{F_{fm}^2\sum_{i=1}^n\tau_i^2}{n\rho^2 c dV^2} + \frac{\lambda\cdot t}{n\rho c}\sum_{i=1}^n\nabla^2(\Delta T_i) + T_0 \end{aligned} \tag{10}$$

The first two terms of eq 10 refer to the temperature rise caused by heat resulting from the conversion of external mechanical energy into internal energy, and the last term refers to the temperature rise caused by heat conduction. Under ideal conditions, there is no external heat exchange in the loading process of coal-rock, so the value of the last term of eq 10 is 0. It can be seen that the temperature rise of coal-rock is only caused by energy conversion. Then, T_{ave} can be obtained as follows:

$$\begin{aligned} T_{ave} &= \frac{F_{fm}a\cdot\tau^2}{cm}\cdot\sigma_{all} - \frac{F_{fm}^2\cdot\tau^2}{cm} + T_0 \\ &= k\cdot\sigma_{all} - b + T_0 \end{aligned} \tag{11}$$

where m is the overall mass of composite coal-rock (kg); a is the average action constant of the crack angle and τ is the effective time of sliding friction (s), both of which are related to material properties; and k and b are thermal constants of composite coal-

https://doi.org/10.1021/acsomega.1c07289
ACS Omega 2022, 7, 8060−8076

rock loading, and their values are only related to material property parameters.

Equation 11 is the temperature−stress coupling model of composite coal-rock, from which it can be seen that the composite stress σ_{all} has a linear relationship with the average body temperature T_{ave} under loading. In eq 11, there are no external parameters representing loading rate, initial confining pressure, and so on for k and b, so it can be seen that the change of external parameters will not affect the stress−temperature linear relationship.

2.2.2. Analysis of Dissipative Energy−Infrared Radiation Energy Relationship. As mentioned above, all objects higher than absolute zero will emit infrared radiation, whose radiation intensity is closely related to material properties and temperature state. During the loading process, the composite coal-rock is heated up due to the work of the external force, some atoms or molecules inside are into excited states by heating, and externally detectable infrared radiation intensity changes. Based on this, the temperature state of coal-rock can be obtained by noncontact measurement of infrared radiation intensity, then the dissipated energy of infrared radiation can be calculated, and finally the state of coal-rock also can be obtained.

The composite coal-rock can be regarded as a kind of gray body material.[54] According to thermodynamics, modern quantum mechanics, and the above analysis, it can be known that the radiation capacity of the composite coal-rock follows the Stefan−Boltzmann law. According to refs 55 and 56, the source of infrared radiant energy is emitted photon energy, and the relation between its radiation capacity E_h and average temperature T_{ave} is

$$E_h = C\left(\frac{T_{ave}}{100}\right)^4 = \varepsilon C_0\left(\frac{T_{ave}}{100}\right)^4 \tag{12}$$

where C is the radiation coefficient of gray body ($W/(m^2 \cdot K^4)$); ε is the blackness of composite coal-rock, which is only related to the property of the material itself, $\varepsilon = E_h/E_b \approx 0.96$; E_b is the radiation capacity of the black body at the same temperature (W/m^2); and C_0 is the black body radiation coefficient, $C_0 = 5.67$ $W/(m^2 \cdot K^4)$.

By combining eq 11 with eq 12, coal-rock's numerical relationship between stress and infrared radiation energy can be obtained, as follows:

$$\begin{cases} E_h = \varepsilon C_0\left(\dfrac{k\cdot\sigma_{all} - b + T_0}{100}\right)^4 \\ k = \dfrac{F_{fm}a\cdot\tau^2}{cm} \\ b = \dfrac{F_{fm}^2\cdot\tau^2}{cm} \end{cases} \tag{13}$$

According to eq 13, the relation between infrared radiation energy and resultant stress σ_{all} is a unary quartic function. For triaxial loading, the resultant stress σ_{all} is deviatoric $(\sigma_1 - \sigma_3)$.

If the composite coal-rock is in an ideal heat insulation environment (there is no external energy exchange), it can be seen from eq 1 that the external mechanical energy W_m will all transform into the internal energy W_i and then finally transform into elastic strain energy W_d or dissipated energy W_d. According to ref 57, the strain energy density U of the coal-rock is calculated by eq 14, as follows:

$$U = U_d + U_e = \sum_{i=1}^{3}\int \sigma_i d\varepsilon_i \tag{14}$$

where σ_i $(i = 1, 2, 3)$ is the triaxial principal stress (Pa); ε_i $(i = 1, 2, 3)$ is the triaxial strain; U_d is the unit dissipated energy, which consists of heat energy, kinetic energy, infrared radiation energy, electromagnetic radiation energy, etc. (J/m^3); and U_e is unit elastic strain energy (J/m^3).

When the composite coal-rock is under triaxial loading, the principal stress in x and y directions is equal $(\sigma_2 = \sigma_3)$. Combined with refs 57−59, the unit elastic strain energy U_e can be calculated as follows:

$$U_e = \frac{1}{2E}[\sigma_1^2 + 2\sigma_3^2 - 2\upsilon\sigma_3(2\sigma_1\sigma_3 + \sigma_3)] \tag{15}$$

where E is the elastic modulus of loading at the elastic stage and υ is Poisson's ratio. Therefore, the calculation formula of unit dissipation energy U_d under triaxial loading is as follows:

$$U_d = \int \sigma_1 d\varepsilon_1 + 2\int \sigma_3 d\varepsilon_3 - \frac{1}{2E}[\sigma_1^2 + 2\sigma_3^2 - 2\upsilon\sigma_3(2\sigma_1\sigma_3 + \sigma_3)] \tag{16}$$

By combining eq 13 and eq 16, the numerical relationship between infrared radiant energy and dissipation energy can be obtained as follows:

$$\begin{cases} ①\sigma_1 = \sigma_3 + \dfrac{1}{k}\left[b - T_0 + 100\left(\dfrac{E_h}{\varepsilon C_0}\right)^{1/4}\right] \\ ②U_d = \displaystyle\int \sigma_1 d\varepsilon_1 + 2\int \sigma_3 d\varepsilon_3 - \frac{1}{2E}[\sigma_1^2 + 2\sigma_3^2 - 2\upsilon\sigma_3(2\sigma_1\sigma_3 + \sigma_3)] \\ ③k = \dfrac{F_{fm}a\cdot\tau^2}{cm}\ ④b = \dfrac{F_f^{m2}\cdot\tau^2}{cm} \end{cases} \tag{17}$$

It can be seen from eq 17 that there is a numerical relationship between the infrared radiant energy E_h and the dissipated energy U_d in the loading process, but it cannot be expressed by a simple linear function, which is different from the relationship between the physical quantity in eq 11. After substituting equations ①, ③, and ④ in eq 17 into ②, there is no parameter of time t or rate v. Therefore, when the initial confining pressure σ_3 is constant, there is a one-to-one correspondence between the dissipated energy U_d and the infrared radiant energy E_h. So, the confining pressure should be kept constant during the loading test.

2.3. Sample Preparation and Experimental Methods. To analyze the coupling law between dissipated energy and infrared radiation energy in the loading process of composite coal-rock mentioned above and to explore the law between energy and fracture, uniaxial and triaxial loading experiments were used to study self-made composite coal-rock. The experimental sample making method and experimental plan are described below.

2.3.1. Sample Making Method and Industrial Analysis of Coal. According to previous research and experience, the samples selected in the experiment should be a "rock-coal-rock" three-layer combination structure. According to the requirements of the International Society of Rock Mechanics for the experiment, the overall sample is processed into a standard cylinder specimen with a diameter of 50 mm and a combined

https://doi.org/10.1021/acsomega.1c07289
ACS Omega 2022, 7, 8060−8076

ratio of 100 mm to 1:1:1. The sample structure is shown in Figure 4.

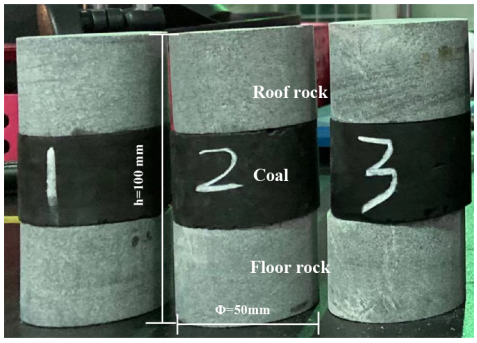

Figure 4. Test sample and size.

As can be seen from Figure 4, the experimental samples are composed of roof rock, coal, and floor rock. The roof rock and floor rock of the test sample are sandstone, and coal seam is taken from a deep coal seam in a mine in Nei Mongol. The source address of experimental coal samples is shown in Figure 5.

Figure 5. Source address of experimental coal samples.

The 5E-MACIII infrared fast coal quality analyzer was used to measure the industrial analysis indexes of three coal seam samples that were identical with the experimental samples. The determination results are shown in Table 1, and *M*, *A*, *V*, and FC in it, respectively, represent moisture, ash, volatile matter, and fixed carbon.

Table 1. Industrial Analysis of Coal Seams

no.	*M* (%)	*A* (%)	*V* (%)	FC (%)
1	5.25	12.74	15.67	66.34
2	5.67	12.58	16.23	65.52
3	5.88	11.96	16.08	66.08
average	5.60	12.43	15.99	65.98

2.3.2. Experimental Conditions and Methods. The uniaxial and triaxial experimental sites are shown in Figure 6, and the structures of the two experimental systems are shown in Figure 7. It can be seen from Figures 6 and 7 that there is little difference between the two experimental scenes. The TAW-2000 triaxial test system was adopted in both of them, which was mainly composed of a computer, power cabinet, rock loading system, and strain sensor. All data during the experiment were timely

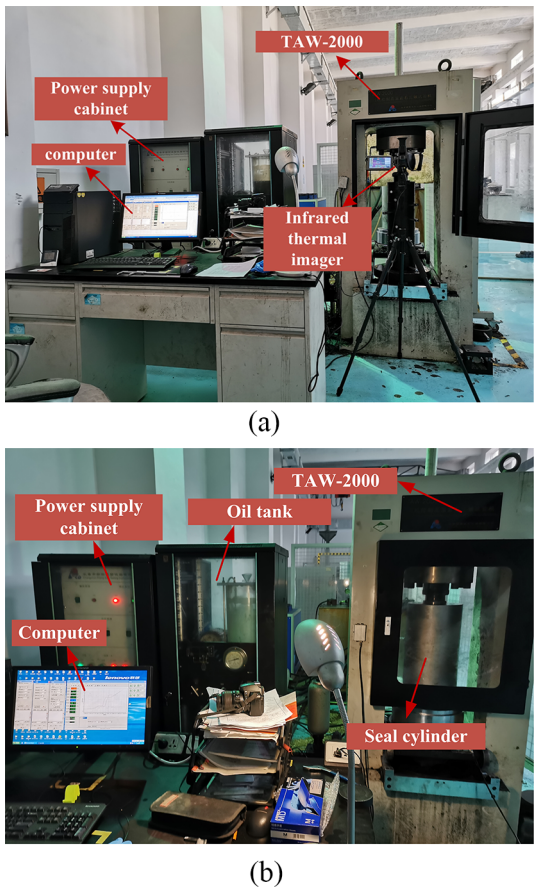

Figure 6. The experiment site. (a) Uniaxial loading scenario. (b) Triaxial loading scenario.

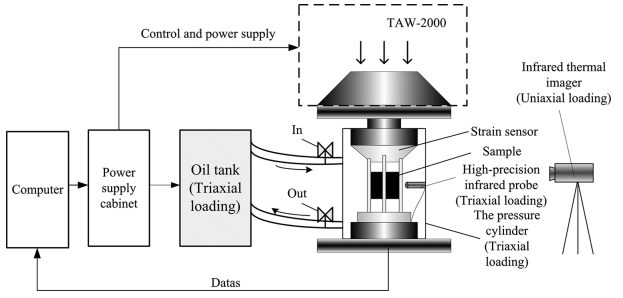

Figure 7. Laboratory equipment.

sent to the computer for storage, which is convenient for subsequent analysis.

The ThermoView TM Pi20 infrared thermal imager was selected for the uniaxial experiment to detect infrared thermal imaging on the surface of the sample during loading, with a sensitivity of 0.03 °C. During the triaxial experiment, the infrared thermal imager cannot detect infrared thermal imaging on the sample surface because of the enclosed pressure cylinder. Infrared radiation is a kind of electromagnetic signal in nature, which also follows the law of electromagnetic propagation. According to the electromagnetic theory and previous studies,[60,61] the electrical conductivity of pressurized oil is extremely low, so it can be known that the infrared radiation propagates in silicone oil with a small energy loss. Therefore, an oil-resistant high-precision infrared probe can be installed in the cylinder to collect the changes of infrared radiation on the

https://doi.org/10.1021/acsomega.1c07289
ACS Omega 2022, 7, 8060−8076

sample surface during loading, and its sensitivity is 0.02 °C. Because the temperature changes weakly during loading, the liquid flow in the constant pressure cylinder may cause temperature loss, thus interfering with the data results. To solve this problem, the following two solutions can be adopted: on the one hand, the infrared probe should be installed as close to the sample as possible; on the other hand, after the confining pressure loading is completed, it should be static for a period of time to make the system relatively stable before the test. In the process of data acquisition, the original data signal must be preprocessed and digital−analog converted by the signal acquisition system so as to facilitate further data analysis and calculation of the computer.

To ensure the universality of experimental results, multiple control groups were set up in each experiment. In the uniaxial loading experiment, nine identical composite coal-rock samples were set up, labeled as D_1−D_9, and then divided into three groups on average. The uniaxial test was carried out according to normal speed, high speed, and fast speed in each group. The uniaxial loading rates of D_1−D_3 were 0.1 mm/min, those of D_4−D_6 were 0.3 mm/min, and those of D_7−D_9 were 1 mm/min. In the triaxial loading experiment, nine identical samples were set up, labeled as S_1−S_9, and divided into three groups. The three groups were subjected to constant triaxial loading according to the three confining pressures of low pressure, medium pressure, and high pressure. The confining pressures of S_1−S_3 were 10 MPa, those of S_4−$_6$ were 15 MPa, and those of S_7−S_9 were 20 MPa.

To determine the coupling relationship between various energies of composite coal-rock under different loading conditions, the study designed two groups of experiments under triaxial and uniaxial loading. In the uniaxial loading experiments, three loading speeds of 0.1, 0.3, and 1 mm/min were set. The same confining pressure was atmospheric pressure in each uniaxial experiment, ensuring a single variable. Under the triaxial loading experiment, three initial confining pressures of 10, 15, and 20 MPa were set. The loading rate of each experiment was 0.1 mm/min, which ensured the single variable of the experiment.

The experimental steps of uniaxial loading are as follows:

(1) The composite coal-rock samples were glued between layers with adhesive tape, and the strain sensor was installed and then fixed on the test machine. The infrared thermal imager was aimed at the center of samples to measure the trend of average surface temperature during loading.

(2) Before starting the experiment, close the equipment unrelated to the experiment, close the laboratory doors, and windows, and stop unnecessary walking.

(3) Power on the experiment and set the loading rate of each group to 0.1, 0.3, and 1 mm/min, respectively. Start the infrared thermal imager first, and then start the press after the indicator becomes stable. Meanwhile, record the surface temperature, stress, and strain in the loading process.

(4) Observe the experimental data until the axial stress exceeds the stress peak and the sample is destroyed. The experiment ends and the data are saved for subsequent processing.

Triaxial loading experiment steps are as follows:

(1) The composite coal-rock samples are glued to each layer with adhesive tape, and strain sensors are installed. Put it into the pressure cylinder, push the pressure cylinder into the tester, and open the oil valve.

(2) Switch on the power supply. First turn on the infrared probe to record the temperature, and then turn on the press after it is stabilized. The triaxial stress σ_1−σ_3 is applied to the predetermined confining pressure value (10, 15, and 20 MPa).

(3) The confining pressure σ_3 is kept constant, and the loading rate is 0.1 mm/min by the displacement control method. Meanwhile, the surface temperature, stress, and strain during the loading process are recorded.

(4) Observe the axial stress in real time. When the axial stress exceeds the stress peak, stop the experiment and save the data for subsequent processing.

After the completion of the above six groups of experiments, physical parameters such as stress, strain, and temperature were converted into total energy, dissipated energy, elastic strain energy, and infrared radiation energy according to eqs 14−16, and then further analysis was conducted. Because the sample components are basically the same and the experimental conditions are the same, the sample data with the most obvious characteristics are selected from the three samples' data in each group for analysis. If the three samples' data in a certain group have high dispersion, it must be supplemented to carry out the experiment under the same loading conditions.

3. RESULTS AND DISCUSSION

3.1. Experimental Results and Fracture State of Samples. Through the uniaxial and triaxial compression experiments mentioned above, energy characteristic parameters of composite coal-rock samples under different loading conditions were obtained, such as stress, strain, sample surface temperature, and so on. Table 2 shows the sizes and experimental results of D_1−D_9, and Table 3 shows S_1−S_9.

Table 2. Uniaxial Specimen Size and Experimental Results

no.	high (mm)	diameter (mm)	loading rate (mm·min^{-1})	compressive strength (MPa)
D_1	101.32	49.64	0.10	29.61
D_2	98.68	49.78	0.10	28.35
D_3	100.24	49.12	0.10	30.47
D_4	101.58	49.84	0.30	23.12
D_5	101.10	50.12	0.30	25.63
D_6	100.74	50.04	0.30	28.47
D_7	98.24	49.78	1.00	31.04
D_8	97.78	49.94	1.00	32.72
D_9	99.64	50.24	1.00	29.33

The results show that the failure trend of nine uniaxial and nine triaxial samples was similar. Therefore, this paper presents

Table 3. Triaxial Specimen Size and Experimental Results

no.	high (mm)	diameter (mm)	confining pressure (MPa)	compressive strength (MPa)	deviatoric stress peak (MPa)
S_1	101.64	49.54	10	46.07	36.07
S_2	101.24	49.54	10	45.50	35.50
S_3	101.10	50.12	10	47.57	37.57
S_4	101.32	49.60	15	68.26	53.26
S_5	100.98	49.58	15	63.12	48.12
S_6	100.74	50.04	15	65.56	50.56
S_7	101.52	49.64	20	76.54	56.54
S_8	101.84	49.82	20	79.37	59.37
S_9	101.62	50.12	20	80.12	60.12

https://doi.org/10.1021/acsomega.1c07289
ACS Omega 2022, 7, 8060−8076

only one failure diagram of uniaxial sample and one failure diagram of triaxial sample. The results are shown in Figure 8. As

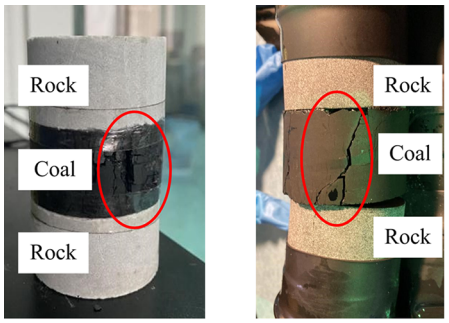

Figure 8. Experimental sample. (a) Result of uniaxial experiment. (b) Result of triaxial experiment.

can be seen from Figure 8, in both uniaxial or triaxial tests, only the coal layer had a penetrating fracture, and the rock was slightly fractured but no obvious fracture was observed. It can be seen that the coal layer of composite coal-rock is more fragile. In addition, the preliminary research results also show that the temperature change of coal is more significant than that of rock during the loading process. To specifically analyze the reasons for the fracture of coal-rock and study the coupling relationship between dissipated energy and infrared radiation energy in the loading process, this paper only measured the average temperature of the coal surface but did not measure the temperature of rock.

3.2. External Factors' Influence on the Relationship between Characteristic Parameters of Energies. *3.2.1. Analysis of the Influence of Loading Rate on the Correlation of Each Energy Characteristic Parameter.* As the experimental results of nine samples in three groups showed the same trend in the uniaxial experiment, only the stress−strain curves and temperature change curves of D_1, D_4, and D_8 are shown in Figure 9. According to previous research results[35] and uniaxial experimental results, all results have the same trend under different loading rates. There are four obvious stages of compaction, elasticity, elastic−plastic stage, and fracture on stress−strain curves of each group under uniaxial loading, and the variation trend of temperature under different loading rates is basically the same.

The loading experiment result curve of conventional speed loading D_1 was taken as an example (Figure 9a) for analysis: In the compaction stage, the temperature of the internal crack closure fluctuated slightly, ranging from 0.01 to 0.03 °C, which was still stable, and infrared radiation energy did not change much. After entering the elastic stage, the temperature began to fluctuate and rise until it entered the elastic−plastic stage. In this process, the temperature rise range was between 0.08 and 0.12 °C, which was significantly larger than that of the previous stage, and infrared radiation energy increased. In elastic−plastic stage, the temperature fluctuated violently between 0.01 and 0.03 °C, the average surface temperature was obviously higher than that in the compaction stage, and the infrared radiation energy had little change. In the fracture stage, the temperature dropped rapidly to the average temperature in the compaction stage, and infrared radiation energy decreased.

It can be seen from Figure 9 that the average surface temperature of coal-rock fluctuates seriously in the loading process, so it is inappropriate to directly merge it with axial stress. Therefore, in this study, the original temperature data were smoothed according to its variation trend before the fitting analysis. And during the loading process, 10−13 strains were selected as intermediate variables to get corresponding temperature and axial stress data. (Each stage should have a certain number of strain sampling points.) Then, linear fitting was carried out for the sampled surface average temperature and axial stress data, and the fitting results are shown in Figure 9 and Table 4. It can be seen from Figure 10 and Table 4 that the surface average temperature of samples under different loading conditions are in a first-order function relationship with stress, and the correlation coefficients of the two are between 0.93 and 0.97. Therefore, it can be seen that there is a strong correlation between temperature and stress, and the loading rate does not affect the correlation trend, which is consistent with the form of eq 11 above.

Table 4. Fitting Results and Correlation Coefficients

no.	fitting relation	correlation coefficient
D_1	$T_{ave} = 0.00242\sigma_1 + 20.6529$	0.9360
D_4	$T_{ave} = 0.00519\sigma_1 + 21.6314$	0.9678
D_8	$T_{ave} = 0.00321\sigma_1 + 19.6618$	0.9433

3.2.2. Analysis of the Influence of Initial Confining Pressure on the Correlation of Each Energy Characteristic Parameter. As the loading conditions of each triaxial test group are the same and the trend is consistent, only the experimental results of S_2, S_4, and S_7 are shown in Figure 11. As can be seen from the

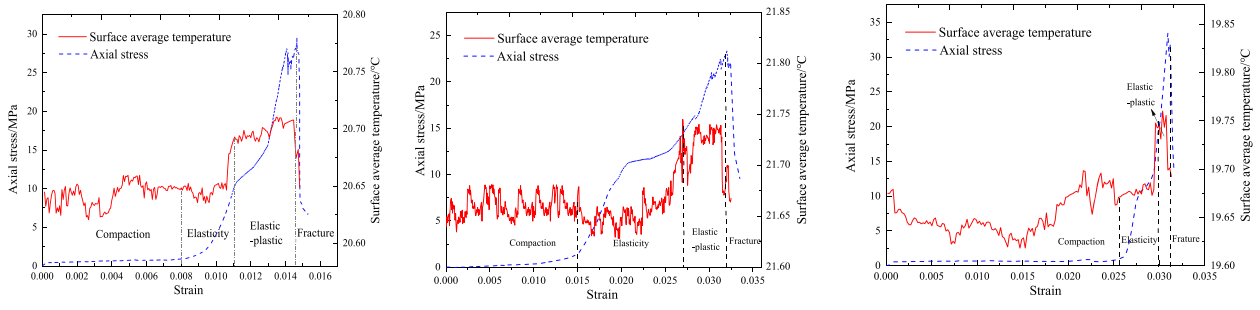

Figure 9. Uniaxial loading experimental result curve. (a) The experimental result of D_1 uniaxial loading at 0.1 mm/min. (b) The experimental result of D_4 uniaxial loading at 0.3 mm/min. (c) The experimental result of D_8 uniaxial loading at 0.3 mm/min.

https://doi.org/10.1021/acsomega.1c07289
ACS Omega 2022, 7, 8060−8076

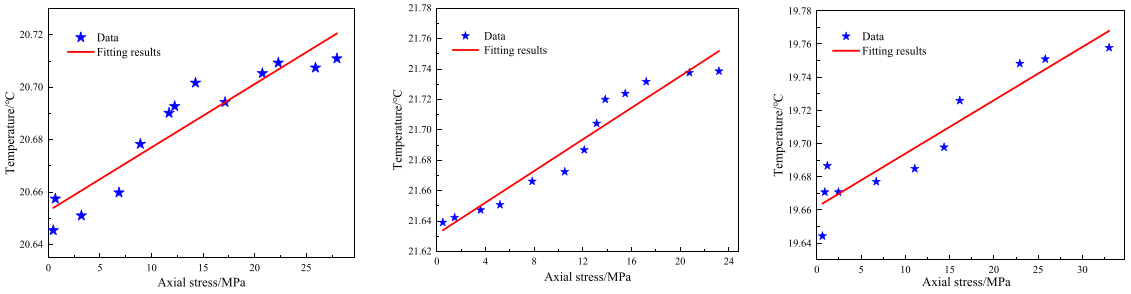

Figure 10. Stress−temperature correlation curve. (a) The fitting results of D_1 uniaxial loading at 0.1 mm/min. (b) The fitting results of D_4 uniaxial loading at 0.3 mm/min. (c) The fitting results of D_8 uniaxial loading at 0.3 mm/min.

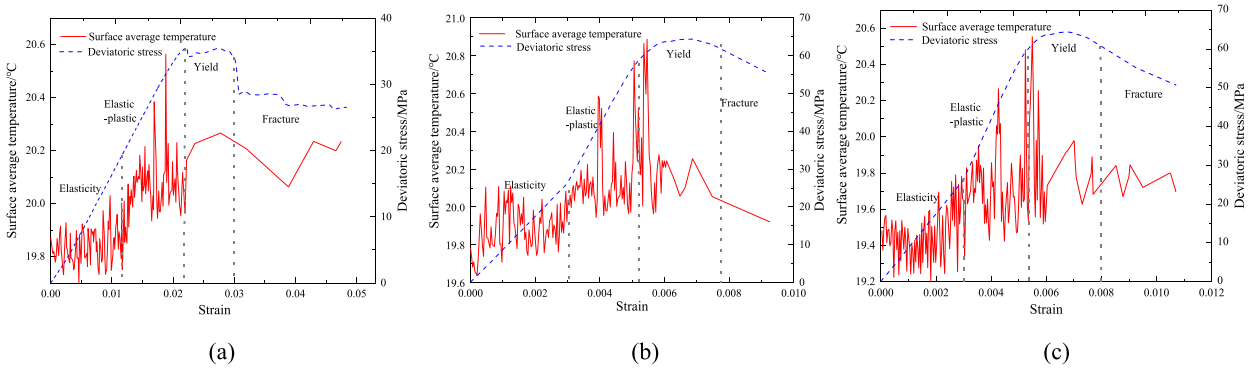

Figure 11. Triaxial loading experimental results curve. (a) The experimental result of S_2 triaxial loading at 10 MPa. (b) The experimental result of S_4 triaxial loading at 15 MPa. (c) The experimental result of S_7 triaxial loading at 15 MPa.

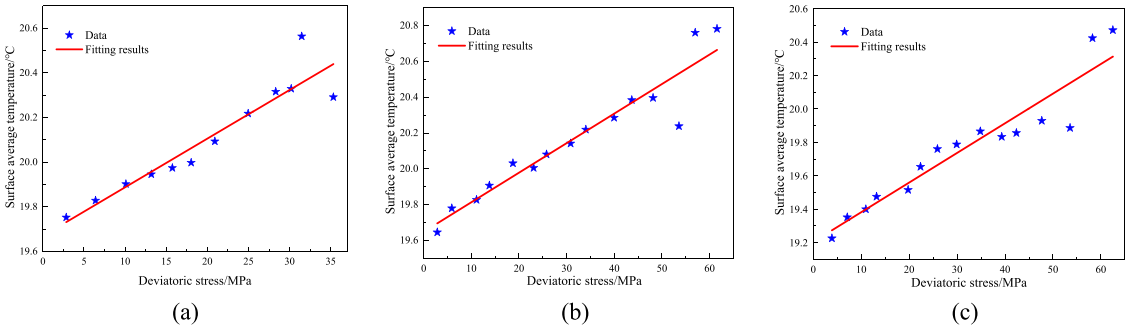

Figure 12. Stress−surface average temperature correlation curve. (a) The fitting results of S_2 triaxial loading at 10 MPa. (b) The fitting results of S_4 triaxial loading at 15 MPa. (c) The fitting results of S_7 triaxial loading at 15 MPa.

experimental results and Figure 11, the surface temperature and deviatoric stress changed in a consistent trend under different loading confining pressures. Because the triaxial test must start from the state of stress balance, there was no compaction stage similar to the uniaxial test, but there were still four stages of elasticity, elastic−plastic stage, yield, and fracture, which also had strong stage characteristics.

As can be seen from Figure 11, changes of surface temperature at different mechanical stages had stage characteristics: At the elastic stage, the temperature fluctuated between 0.10 and 0.15 °C, which was more violent than that of uniaxial loading, and the overall trend was relatively stable. In the elastic−plastic stage, because the sample was a composite material, the increase rate of deviational stress was larger than that in the previous stage.[15] In this stage, the temperature fluctuated rapidly and rose sharply in the early stage, the average temperature was obviously higher than that in the elastic stage, and an obvious peak of temperature appeared before the yield stage. The duration of the yield stage was very short. In this stage, the temperature of the sample surface still kept a rising trend for a period of time, but it was not violent, and at the later stage, it showed a rapid downward trend.

According to the comparison of Figures 9 and 11, the variation trend of surface average temperature of composite coal-rock during triaxial loading was similar to that of uniaxial loading, and the temperature peak was slightly earlier than the stress peak. In addition, there was a high similarity between the deviatoric stress and temperature. The fitting curves of Figure 12 were obtained from the numerical fitting of axial stress and temperature in Figure 11. And the data processing method before fitting is similar to that in Figure 10. The fitting results are shown in Table 5. It can be seen from Figure 12 and Table 5 that the surface average temperature of samples under different initial confining pressures are in a first-order function relationship with stress, and the correlation coefficients of the two are between

https://doi.org/10.1021/acsomega.1c07289
ACS Omega 2022, 7, 8060−8076

Table 5. Fitting Results and Correlation Coefficients

no.	fitting relation	correlation coefficient
S_2	$T_{ave} = 0.02179(\sigma_1-\sigma_3) + 19.6697$	0.9414
S_4	$T_{ave} = 0.01651(\sigma_1-\sigma_3) + 19.6482$	0.9512
S_7	$T_{ave} = 0.01774(\sigma_1-\sigma_3) + 19.2048$	0.9463

0.94 and 0.95. It can be seen that the initial confining pressure does not affect the first-order function relation of correlation, which is consistent with eq 11.

Based on the above experimental analysis, it can be seen that there is basically a linear relationship between the composite coal-rock stress and the average surface temperature under different loading conditions, and the fitting degree is higher than 0.93, which is consistent with the description of eq 11 in Section 2.2. Based on the derivation of eq 17 in Section 2.2, it can be seen that the rationality of eq 17 is based on the establishment of eqs 11, 12, and 16. And the rationality of eqs 12 and 16 has been verified in other existing literatures. On the basis of and in combination with the experimental analysis in this section, the correctness of eq 11 is similarly verified. Thus, the rationality of eq 17 has been verified indirectly.

3.3. Establishment of the Composite Coal-Rock Energy Coupling Mechanism during the Loading Process. *3.3.1. Analysis of Total Energy Conversion Trend in the Loading Process.* The deformation of composite coal-rock under load is closely related to the energy conversion. As shown in eq 14, in the absence of other exchanges, all the work done by the external environment is transformed into elastic strain energy and dissipation energy. Figure 13a–c shows the variation curves of total energy, dissipated energy, elastic strain energy, and strain of D_1, D_4, and D_8 at uniaxial loading rates of 0.1, 0.3, and 1 mm/min, respectively, as well as stress–strain curves. It can be seen from Figure 13a–c that the total energy of composite coal-rock under the uniaxial condition was transformed into various energies in different mechanical stages according to different laws, and the loading rate did not affect the energy transformation trend at each stage.

As the trend of all curves was consistent, only Figure 13a was used for specific analysis below: In the compaction stage, more than 99% of the total energy was converted to elastic strain energy; however, the part that was converted into dissipated energy was very little. The total energy increased slowly, which was similar to the change trend of stress. In this stage, the energy was mostly elastic deformation, and the total energy density reached 4.757 mJ/mm^3 at the end. At the elastic stage, the total energy increased rapidly, and the growth rate reached 24.3738 mJ/mm^3 later. At this stage, most of the total energy was still converted into elastic strain energy, but the growth rate was significantly lower than that of the total energy, and the conversion rate gradually decreased, while the conversion dissipation energy increased significantly, but the total energy did not exceed the elastic strain energy. At the end of this stage, the energy density of both was 12.788 mJ/mm^3. At this time, the external work was still mostly used for elastic deformation, but due to the complex internal structure of materials, some areas had reached the elastic limit. As the loading process progresses, the inelastic proportion area of samples increased, and part of the total energy was converted into dissipated energy to be consumed. In the elastic–plastic stage, the total energy kept increasing at a high rate. In the early part of this stage, the elastic strain energy and dissipation energy increased almost at the same rate, with a growth rate of 6931.394 mJ/mm^3, which was significantly higher than that in the previous stages. In addition,

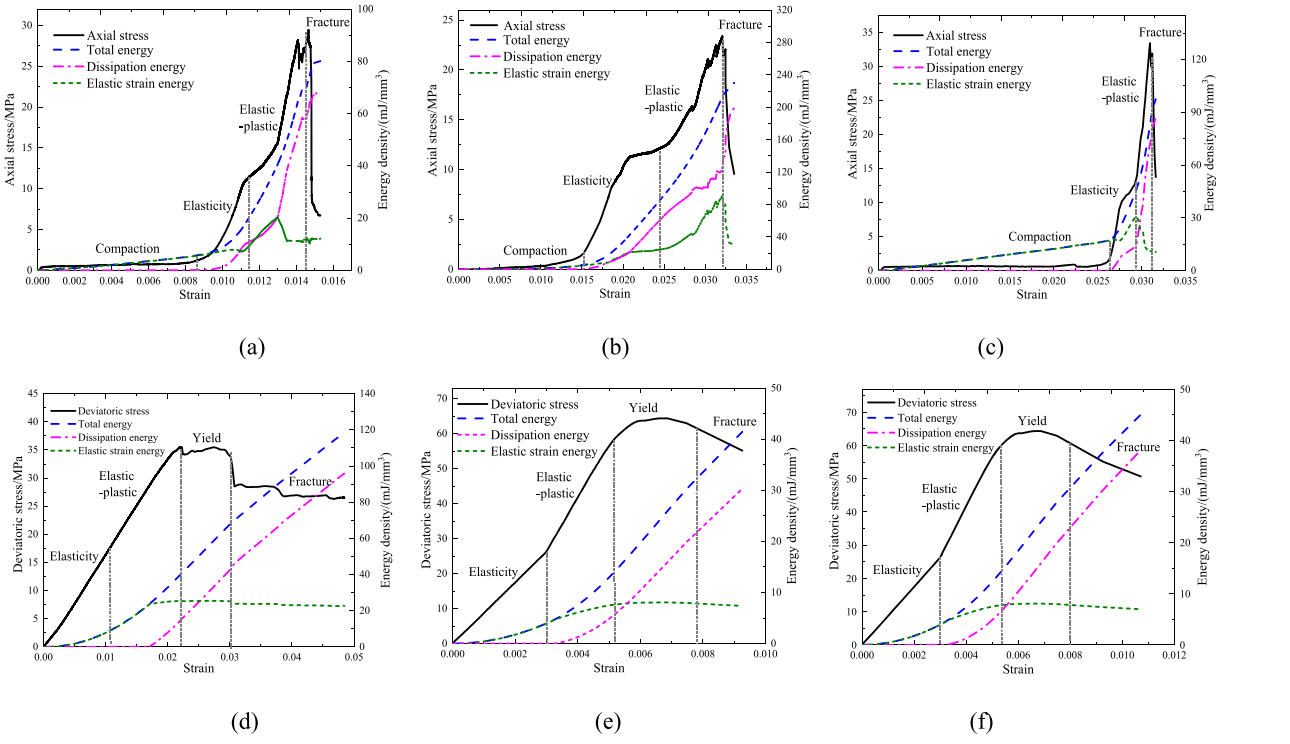

Figure 13. Energy change curve in the loading process. (a) The energy change curve with a uniaxial loading rate of 0.1 mm/min. (b) The energy change curve with a uniaxial loading rate of 0.3 mm/min. (c) The energy change curve with a uniaxial loading rate of 1 mm/min. (d) The energy change curve of the initial confining pressure of 10 MPa under triaxial loading. (e) The energy change curve of the initial confining pressure of 15 MPa under triaxial loading. (f) The energy change curve of the initial confining pressure of 20 MPa under triaxial loading.

https://doi.org/10.1021/acsomega.1c07289
ACS Omega 2022, 7, 8060–8076

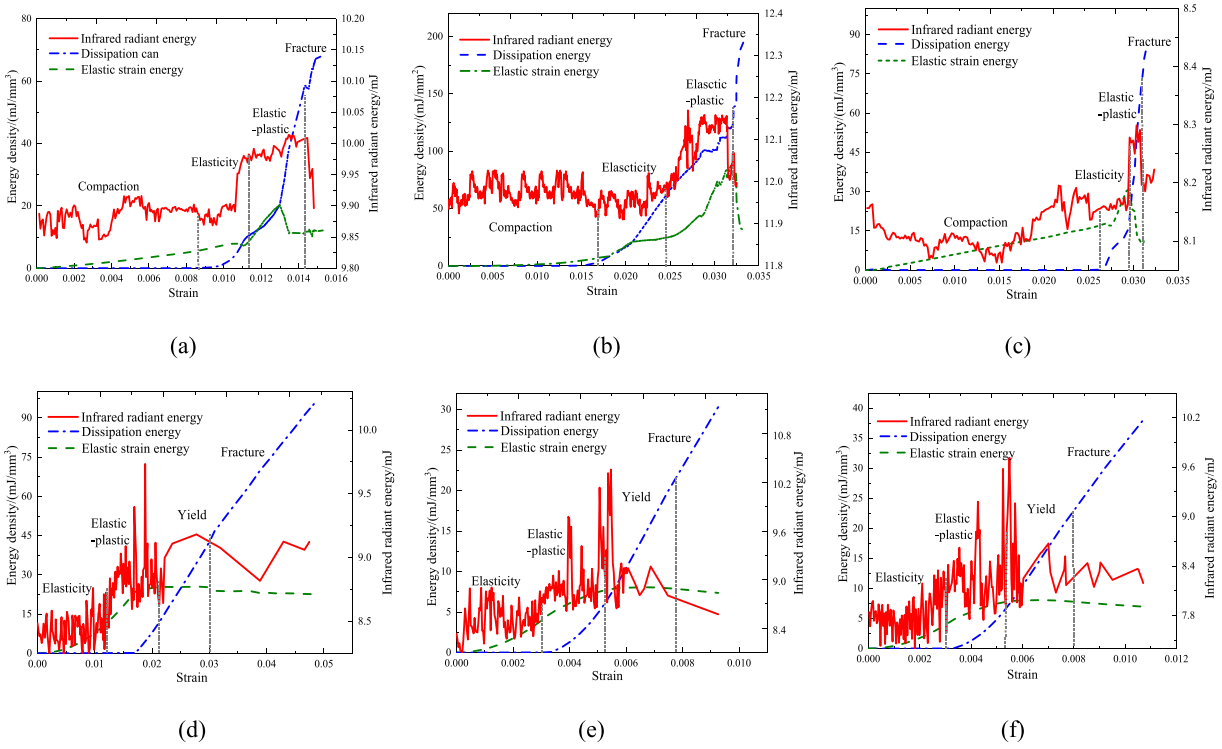

Figure 14. The curve of infrared radiation energy in loading. (a−c) The variation trend of energy density, infrared radiation energy, and strain of composite coal-rock under uniaxial loading rates of 0.1, 0.3, and 1 mm/min, respectively. (d−f) The variation trends of energy density, infrared radiation energy, and strain of the samples under confining pressures of 10, 15, and 20 MPa, respectively.

the conversion ratio of the two energies was the same until the strain reached 0.013. At this point, the elastic strain energy reached the energy peak, and its value was 19.575 mJ/mm^3. It can be seen that there was an energy crossing point at which the elastic strain energy and dissipated energy had the same value and appeared earlier than the stress peak. The total energy conversion trend changed after this point. At this time, the elastic strain energy decreased rapidly, while the dissipated energy density increased, with the growth rate being 23976.865 mJ/mm^3. The total energy and excess elastic strain energy were almost all converted to dissipative energy. And the energy density of elastic strain energy was stable at 11.352 mJ/mm^3 before coal-rock fracture. It can be seen that although the specimen was still mainly elastic deformation in the early elastic−plastic stage, it would eventually reach a limit. The inelastic region continued to increase with the loading and eventually became dominant, which led to the release of most of the remaining energy into dissipative energy. At this time, the sample had a tendency to partially rupture and the sound of rupture could be heard outside. When entering the fracture stage, the elastic strain energy of the sample remained stable, and the total energy almost changed to dissipative energy, which still kept a high growth rate. Finally, the dissipated energy reached the energy peak of 68.046 mJ/mm^3, the sample broke, and the dissipated energy was released.

Figure 13d,e shows the variation curves of total energy, dissipated energy, elastic strain energy, and strain of samples S_2, S_4, and S_7 under triaxial loading at confining pressures of 10, 15, and 20 MPa, respectively, as well as the deviant stress−strain curves. It can be seen from Figure 13d,e that the relationship between stress state and energy of composite coal-rock under triaxial loading is similar to that under uniaxial shown in Figure 13a-c, and the total energy is transformed into different energy trends at different mechanical stages. The total energy transformation rule of the triaxial is similar to that of the uniaxial. Because the triaxial stress balance needs to be loaded before the triaxial loading, there is no compaction stage in Figure 13d,e. Figure 13e is taken as an example for specific analysis below: At the elastic stage, the total energy increased at the rate of 2118.563 mJ/mm^3, and almost all the external work was converted to elastic strain energy, while the dissipation energy could be ignored because of the low conversion rate. At this moment, the elastic deformation of the sample could be seen externally. In the elastic−plastic stage, the total energy increased rapidly and the rate increased to 3513.290 mJ/mm^3. Meanwhile, elastic strain energy kept increasing slowly but the growth rate decreased and it gradually approached the energy peak of 24.319 mJ/mm^3. In this stage, the total energy was transformed into dissipated energy at a faster speed, which was similar to the early elastic−plastic stage of uniaxial. However, the elastic strain energy still existed in a large amount inside the specimen, so the outer part of the specimen was still elastic deformation, but the inner part had a plastic deformation trend. At the initial stage of yield, the total energy conversion dissipation energy kept increasing, the elastic strain energy was almost stable at 7.558 mJ/mm^3, and the energy density was 25.402 mJ/mm^3 when the strain was 0.0056, which was earlier than that of stress. Since then, almost all the total energy was converted to dissipative energy, and part of elastic strain energy was also converted to it, which led to the rapid growth of dissipative energy until rupture. This stage was the same as the later stage of the uniaxial loading elastic−plastic stage. The plastic deformation trend of the sample was gradually greater than the elastic, and finally, the specimen cracked because the plastic deformation reached the load strength. To sum up, under triaxial loading, there is a corresponding relationship between energy transformation

https://doi.org/10.1021/acsomega.1c07289
ACS Omega 2022, 7, 8060−8076

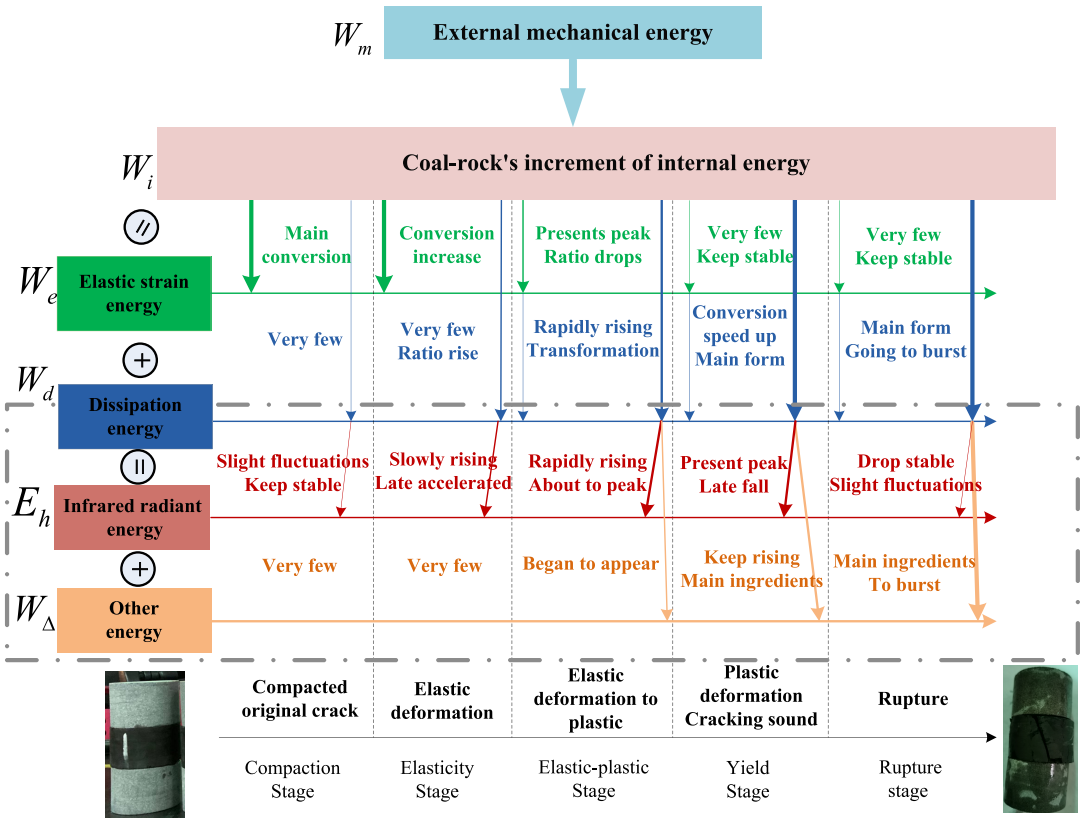

Figure 15. A method to judge the state of coal-rock by the coupling relation of dissipated energy and infrared radiation energy.

trend and stress. Before the rupture, it has the same characteristics as the uniaxial one; that is, the dissipated energy increases significantly and the elastic strain energy remains stable. Therefore, it is feasible to predict the trend of coal-rock rupture by using energy characteristics.

3.3.2. Trend Analysis of Infrared Radiant Energy and Establishment of Its Coupling Mechanism with Dissipative Energy. According to the above analysis, the change of energy state of composite coal-rock during loading can be expressed by eq 1, and infrared radiant energy is one of the components of dissipated energy. According to eq 1, the dissipated energy can be expressed as infrared radiant energy E_h and dissipated energy excluding infrared radiant energy W_Δ. Thus, eq 1 can be processed to obtain the relation of eq 18, as follows:

$$\begin{cases} E_h \propto U_h \\ U_d(\sigma_1, \sigma_3) = U_h(\sigma_1, \sigma_3) + U_\Delta \end{cases} \quad (18)$$

where E_h is infrared radiant energy (J); U_h is infrared radiant energy density, which is proportional to the infrared radiant energy under the same volume (J/m^3); and U_Δ is the energy density of dissipated energy excluding infrared radiant energy (J/m^3).

According to eq 18, when the sample volume is certain, the infrared radiation energy of the object is proportional to the infrared radiation energy density, and the variation trend of the infrared radiation energy E_h is consistent with that of the infrared radiation energy density U_h. Therefore, the variation law of energy density can be obtained by analyzing the variation of infrared radiation energy, which is helpful for the in-depth analysis of the relationship between infrared radiation energy, dissipated energy, and total energy. The infrared radiation energy of composite coal-rock under uniaxial and triaxial loading can be obtained by calculation using eq 12. Since each sample has the same variation trend under the same loading condition, only uniaxial D_1, D_4, and D_8 and triaxial S_2, S_4, and S_7 were analyzed. Figure 14 shows the curves of energy density and infrared radiation energy of the six samples changing with strain.

According to the analysis of Figures 9 and 11 above, it can be seen that the trend of temperature on the sample surface corresponds to each mechanical stage. In addition, it can be seen from Figure 14 that the variation trend of infrared radiation energy and temperature of coal-rock under uniaxial or triaxial loading is basically consistent, which has similar characteristics in various mechanical stages under uniaxial or triaxial loading. To summarize the variation characteristics of various mechanical stages of infrared radiation energy in the loading process, the stress increase process in the early uniaxial elastic−plastic stage is referred to as the elastic−plastic stage, and the transient stress fluctuation in the later stage is referred to as the yield stage. Although coal-rock fracture is a way of releasing dissipative energy, it is very unlikely to directly measure it. As one of the forms of dissipative energy, infrared radiation energy can be measured without contact, which is helpful to judge the state of samples.

It can be seen from Figure 14 that infrared radiation energy was correlated with the variation trend of dissipated energy. Figure 14a under the uniaxial condition and Figure 14e under the triaxial condition were taken as examples for analysis. In the compaction and elastic stages, the total energy was mainly elastic deformation energy. Although the dissipative energy increased slowly, there was no obvious increase trend in general. Meanwhile, the infrared radiation energy changed steadily. At this stage, two energies remained stable at 9.869 and 8.521 mJ,

https://doi.org/10.1021/acsomega.1c07289
ACS Omega 2022, 7, 8060−8076

respectively. At the later stage, the dissipated energy began to rise, and the infrared radiation energy increased slowly in accordance with it. At the early stage of the elastic−plastic phase, the dissipative energy began to increase significantly, and the growth rate under uniaxial and triaxial loading was 5826.818 and 3772.337 mJ/mm^3, respectively. At this time, the infrared radiation energy increased significantly and obvious stages appeared, consistent with the change of dissipative energy. Near the intersection point of elastic strain energy and dissipative energy, the dissipative energy increased rapidly and nearly linearly, the infrared radiation energy increased to a high energy value (9.996 mJ under the uniaxial condition and 9.796 mJ under the triaxial condition), and the infrared radiation energy peak appeared. According to the law of energy conservation and the curve change in Figure 14, the infrared radiation energy at this time came from two parts, mainly from the dissipated energy converted and the transformation of elastic strain energy, which resulted in the sharp increase and high energy peak of infrared radiation energy. In the yield stage, the total energy was mainly transformed into dissipative energy release rather than elastic strain energy. Although the infrared radiation energy still kept the high energy value fluctuation at the early part of this stage, the drop occurred significantly earlier than the stress peak and fracture stage. Combined with the analysis of eq 18, when the proportion of the infrared radiation energy of the dissipated energy begins to decline significantly, the proportion of dissipated energy excluding infrared radiant energy U_Δ (i.e., kinetic energy, plastic deformation energy, etc.) will rise significantly, and the composite coal-rock will begin to enter the fracture deformation stage. At this time, the fracture sound of the sample could be heard externally and cracks could be produced until the penetrating cracks occurred. Therefore, in the late yield and fracture stage, the dissipation energy realization form changed, and the infrared radiation energy was no longer dominant, which fluctuated stably with a low energy value without an increasing trend. At this time, the dissipated energy excluding infrared radiant energy was dominant, leading to fracture.

To sum up, infrared radiant energy is closely related to dissipated energy in the loading process. It also can be seen that the change trend of dissipated energy can be obtained by analyzing the change of infrared radiation energy, and the stress state of composite coal-rock samples can be further obtained. Finally, noncontact prediction of coal-rock state can be achieved by monitoring infrared radiation energy. The method to judge the state of composite coal-rock by using the coupling mechanism of dissipated energy and infrared radiation energy is shown in Figure 15. The thickness of the shear head represents the amount of energy obtained by the conversion.

As can be seen from Figure 15, in the loading process, the internal energy of composite coal-rock will increase due to the action of external mechanical energy. And the increased internal energy will be further transformed into elastic deformation energy and dissipation energy. However, the trend of coal-rock internal energy transformation is different in each loading stage. In the early loading stage, the increment of internal energy W_i is mostly converted to elastic strain energy W_e but rarely to dissipated energy W_d. However, from the elastic−plastic stage, the elastic strain energy W_e of coal-rock basically reaches the upper limit, which leads to the residual internal energy increment W_i and part of elastic strain energy W_e conversion into dissipated energy W_d. It also can be seen from Figure 15 that the change of dissipated energy W_d has an obvious corresponding relationship with the state of composite coal-rock. When the dissipated energy W_d increases rapidly, the fracture process of coal-rock accelerates obviously.

According to eq 1 and Figure 15, dissipative energy can be considered in two forms, one of which is infrared radiant energy and the other is other energy, and at different stress stages, the main forms of dissipated energy are different. Before the elastic−plastic stage, the main form of dissipated energy is infrared radiation energy, and the growth trend of it is almost the same as that of dissipated energy. At this time, based on the above analysis, the composite coal-rock mainly has elastic deformation, the fracture trend is not obvious, and there is no obvious crack outside. After this stage, the form of dissipation energy changes: the proportion of infrared radiation energy decreases, while the other forms of energy increases. Although the infrared radiation energy still keeps increasing in a short time, it tends to saturate obviously. In addition, the performance of other forms of energy is more obvious, and the coal-rock begins the plastic deformation and the production of visible cracks. Finally, before the fracture, the infrared radiation energy decreases rapidly, but the dissipation energy increases rapidly, and other forms of energy increase obviously, which lead to the fracture of the sample.

It can be seen that there is an obvious coupling relationship between infrared radiation energy and dissipated energy, and the dissipated energy state that is difficult to be measured directly can be understood by analyzing the infrared radiation energy state. On this basis, the stress state of coal-rock can be obtained by using this relationship.

At present, contact detection is still the main method to predict the fracture trend of composite coal-rock. Although some studies have used energy theory to predict the failure state, most of them are based on the analysis of elastic strain energy and dissipated energy and rarely involve the analysis of the specific expression form of dissipated energy. So, the relationship between infrared radiant energy and dissipated energy constructed in Figure 15 can provide new ideas for the research in this field and is conducive to further research on noncontact coal-rock fracture state prediction technology.

4. CONCLUSIONS

(1) This paper analyzes the transformation mechanism of various energies and the generation mechanism of infrared radiation energy in the loading process of composite coal-rock from a microscopic perspective. Based on the theory of friction heat generation and heat conduction, the mathematical model of energy characteristic parameters is established by using the method of micro element analysis. On this basis, the coupling model of dissipated energy and infrared radiation energy is further deduced and established based on the thermodynamics theory and Stefan−Boltzmann law.

(2) The variation of dissipated energy in the loading process of composite coal-rock has stages. In the early stages of loading, the dissipation energy obtained by energy conversion is small, but it increases rapidly in the late stages, which causes the rupture of the coal-rock. And the components of dissipated energy are different at different stages, which are closely related to the deformation state of coal-rock.

(3) There is correlation between the variation of infrared radiation energy and dissipation energy. In the early stage, the trend of the two is basically the same, but in the late stage, the infrared radiation energy does not increase significantly, which is different from the trend of dissipation energy. In addition, the

https://doi.org/10.1021/acsomega.1c07289
ACS Omega 2022, 7, 8060−8076

infrared radiation energy drops obviously earlier than coal-rock fracture, which has a certain precursor. Based on this, the relationship between infrared radiation energy and dissipated energy is established, and the change rule of coal-rock state based on energy transformation is further obtained. It will provide a new method to prevent coal-rock dynamic disaster.

AUTHOR INFORMATION

Corresponding Authors

Hao Li − *College of Electrical and Engineering Control, Liaoning Technical University, Huludao 125105, China*; orcid.org/0000-0002-8020-9220; Email: lntulh@foxmail.com

Zhen Yang − *College of Electrical and Engineering Control, Liaoning Technical University, Huludao 125105, China*; Email: yangzhen1980219@163.com

Authors

Xin Li − *College of Electrical and Engineering Control, Liaoning Technical University, Huludao 125105, China*

Hui Zuo − *College of Electrical and Engineering Control, Liaoning Technical University, Huludao 125105, China*

Weiman Sun − *College of Electrical and Engineering Control, Liaoning Technical University, Huludao 125105, China*

Hongzhu Li − *College of Electrical and Engineering Control, Liaoning Technical University, Huludao 125105, China*

Yan Li − *College of Electrical and Engineering Control, Liaoning Technical University, Huludao 125105, China*

Complete contact information is available at: https://pubs.acs.org/10.1021/acsomega.1c07289

Notes

The authors declare no competing financial interest.

ACKNOWLEDGMENTS

This work was supported by the discipline innovation team of Liaoning Technical University (LNTU20TD-29), Chinese National Natural Science Foundation (51604141 and 51204087), Liaoning Provincial Education Committee Projects (LJ2020JCL020), and Natural Science Foundation of Liaoning Province (20170540427).

NOMENCLATURE

W_m	total energy of work done by an external force
W_i	the increased internal energy
E_h	infrared radiation energy converted in the process
W_Δ	the energy form of dissipated energy except infrared radiation energy
T_{in}	internal temperature
T_{out}	external temperature
Q_i	increase in internal energy by No.i unit volume of coal-rock
Q_f	increase in internal energy by converting work done by an external force
Q_a	the increase in internal energy by heat conduction
ΔTi	rising temperature of No.i coal-rock unit
λ	thermal conductivity coefficient of coal-rock
∇^2	Laplacian operator
σ_{all}	combined stress in the original fracture space of the No.i coal-rock unit
dS	unit area of friction surface
θ	angle between the resultant force and the direction of the original crack
τ_i	effective time of sliding friction action of internal cracks
dm	unit mass
dt	unit time
q_i	heat source intensity of No.i coal-rock unit
ρ	density of coal-rock
c	specific heat capacity of coal-rock
dV	unit volume
T_i	temperature of No.i coal-rock unit
T_0	initial temperature of coal-rock
T_{ave}	the average temperature
k	thermal constant of composite coal-rock loading
b	thermal constant of composite coal-rock loading
C	radiation coefficient of the gray body
ε	blackness of composite coal-rock
E_b	radiation capacity of the black body
C_0	black body radiation coefficient
F_{fm}	maximum static friction force
W_e	elastic strain energy
W_d	dissipation energy
σ_i	triaxial principal stress (i = 1, 2, 3)
ε_i	triaxial strain (i = 1, 2, 3)
U_d	unit dissipated energy
U_e	unit elastic strain energy
E	the elastic modulus of loading at the elastic stage
υ	Poisson's ratio
M	moisture
A	ash
V	volatile matter
FC	fixed carbon
U_h	infrared radiation energy density
U_Δ	the energy density of dissipated energy excluding infrared radiant energy

REFERENCES

(1) Lu, J.; Zhang, D.; Huang, G.; Li, X.; Gao, H.; Yin, G. Effects of loading rate on the compound dynamic disaster in deep underground coal mine under true triaxial stress. *Int. J. Rock Mech. Min.* **2020**, 104453.

(2) Jia, Z.; Xie, H.; Zhang, R.; Li, C.; Wang, M.; Gao, M.; Zhang, Z.; Zhang, Z. Acoustic emission characteristics and damage evolution of coal at different depths under triaxial compression. *Int. J. Rock Mech. Rock Eng.* **2020**, *53*, 2063−2076.

(3) Jia, J. C.; Gong, Z. W.; Jin, D. W.; Li, Q. X.; Wu, Y. The main progress in the 13th five-year plan and the prospect of coal geology. *Coal Geol. Explor.* **2021**, *49*, 32−44.

(4) Du, J.; Chen, J.; Pu, Y.; Jiang, D.; Chen, L.; Zhang, Y. Risk assessment of dynamic disasters in deep coal mines based on multi-source, multi-parameter indexes, and engineering application. *Process Saf. Environ. Prot.* **2021**, *155*, 575−586.

(5) Li, Y.; Zhou, L.; Li, D.; Zhang, S.; Tian, F.; Xie, Z.; Liu, B. Shale Brittleness Index Based on the Energy Evolution Theory and Evaluation with Logging Data: A Case Study of the Guandong Block. *ACS Omega* **2020**, *5*, 13164−13175.

(6) Li, D.; Zhang, J.; Sun, Y.; Li, G. Evaluation of rockburst hazard in deep coalmines with large protective island coal pillars. *Nat. Resour. Res.* **2021**, *30*, 1835−1847.

(7) Wu, G.-s.; Yu, W.-j.; Zou, J.-p.; Li, C.-y.; Li, J.-h.; Du, S.-h. Experimental investigation on rockburst behavior of the rock-coal-bolt specimen under different stress conditions. *Sci. Rep.* **2020**, 1.

(8) Zhang, Q.; Wang, E.; Feng, X.; Wang, C.; Qiu, L.; Wang, H. Assessment of rockburst risk in deep mining: an improved comprehensive index method. *Nat. Resour. Res.* **2021**, *30*, 1817−1834.

(9) Wojtecki, Ł.; Iwaszenko, S.; Apel, D. B.; Cichy, T. An attempt to use machine learning algorithms to estimate the rockburst hazard in underground excavations of hard coal mine. *Energies* **2021**, 6928.

(10) Gong, S.-y.; Li, J.; Ju, F.; Dou, L.-m.; He, J.; Tian, X.-y. Passive seismic tomography for rockburst risk identification based on adaptive-

grid method. *Tunnelling. Underground Space Technol.* **2019**, *86*, 198−208.
(11) Gao, W.; Cui, T.; Xiao, T.; Chen, X.; Zhou, C.; Hu, C. J. Crack initiation of rock based on the minimum plastic zone radius criterion. *J. China Coal Soc.* **2021**, *46*, 3193−3202.
(12) Liu, G.; Karakus, M.; Mu, Z. Propagation and attenuation characteristics of rockburst-induced shock waves in coal-rock medium. *Arab. J. Geosci.* **2019**, 113.
(13) Li, X.; Li, H.; Yang, Z.; Sun, Z.; Zhuang, J.; Song, C.; Wang, X. Experimental study on triaxial unloading failure of deep composite coal-rock. *Adv. Civ. Eng.* **2021**, DOI: 10.1155/2021/6687051.
(14) Li, X.; Li, H.; Yang, Z.; Su, X. P.; Ma, Z. Y. Temperature, stress, electromagnetic multifield coupling mechanism of composite coal-rock deformation and fracture. *J. China Coal Soc.* **2020**, *45*, 1764−1772.
(15) Li, X.; Li, H.; Yang, Z.; Wang, X.; He, W. Numerical simulation case study by using FLAC^{3D} of the composite coal-rock on the load-free fracture. *J. Saf. Environ.* **2020**, *20*, 2187−2195.
(16) Liu, X.; Zhang, Z.; Wang, E.; Wang, X.; Yang, B.; Wang, H. Characteristics of electromagnetic radiation signal of coal and rock under uniaxial compression and its field application. *J. Earth Syst. Sci.* **2020**, DOI: 10.1007/s12040-019-1309-0.
(17) Zheng, K. H.; Qiu, B. J.; Wang, Z. Y.; Li, J. P.; Gao, K. Modelling heterogeneous coal-rock (HCR) failure patterns under dynamic impact loads using image-based finite element (FE) and discrete element (DE) model. *Powder Technol.* **2020**, *360*, 673−682.
(18) Guo, J. Y.; Zhang, Y. Z. Analysis on acoustic emission characteristics of coal under uniaxial compression. *Coal Technol.* **2021**, *40*, 129−132.
(19) Li, L.; Liu, Y.; Liu, W.; Zhang, X.; Chen, J.; Jiang, D.; Fan, J. Crack evolution and failure modes of shale containing a pre-existing fissure under compression. *ACS Omega* **2021**, *6*, 25461−25475.
(20) Wu, N.; Liang, Z.; Zhou, J.; Zhang, L. Energy evolution characteristics of coal specimens with preformed holes under uniaxial compression. *Geomech. Eng.* **2020**, *20*, 55−56.
(21) Xue, Y.; Ranjith, P. G.; Dang, F.; Liu, J.; Wang, S.; Xia, T.; Gao, Y. Analysis of deformation, permeability and energy evolution characteristics of coal mass around borehole after excavation. *Nat. Resour. Res.* **2020**, *29*, 3159−3177.
(22) Yang, L.; Gao, F. Q.; Wang, X. Q. Mechanical response and energy partition evolution of coal-rock combinations with different strength ratios. *Chin. J. Rock Mech. Eng.* **2020**, *39*, 3297−3305.
(23) Li, L. P.; Pan, Y. S. Experimental research on energy characteristics of anomalously low friction effect in deep coal and rock mass. *J. China Coal Soc.* **2020**, *45*, 202−210.
(24) Duan, M. K.; Jiang, C. B.; Gan, Q.; Li, M. H.; Peng, K.; Zhang, W. Z. Experimental investigation on the permeability, acoustic emission and energy dissipation of coal under tiered cyclic unloading. *J. Nat. Gas Sci. Eng.* **2020**, *73*, 103054.
(25) Li, X. L.; Chen, S. J.; Wang, E. Y.; Li, Z. H. Rockburst mechanism in coal rock with structural surface and the microseismic (MS) and electromagnetic radiation (EMR) response. *Eng. Fail. Anal.* **2021**, *124*, 105396.
(26) Xue, Y.; Cao, Z. Z.; Li, Z. H. Destabilization mechanism and energy evolution of coal pillar in rockburst disaster. *Arab. J. Geosci.* **2020**, *13*, 1.
(27) Mohammadali, S.; Derek, B. A.; Samer, A.; Paul, L.; Robert, A. H. Evaluation of mining-induced energy and rockburst prediction at a diamond mine in Canada using a full 3D elastoplastic finite element model. *Eng. Geol.* **2020**, *266*, 105457.
(28) Yang, L.; Gao, F. Q.; Wang, X. Q.; Li, J. Z. Energy evolution law and failure mechanism of coal-rock combined specimen. *J. China Coal Soc.* **2019**, *44*, 3894−3902.
(29) Li, B.; Zhang, Y.; Ren, C.; Yang, K.; Li, J.; Xu, J. Energy characteristics of coal or rock damage under thermo-mechanical coupling effect. *China Saf. Sci. J.* **2019**, *29*, 91−96.
(30) Wang, F.-K.; Wu, C.-T. M.; Horng, T.-S.; Tseng, C.-H.; Yu, S.-H.; Chang, C.-C.; Juan, P.-H.; Yuan, Y. Review of self-injection-locked radar systems for noncontact detection of vital signs. *IEEE J. Electromagn., RF and Microwaves Med. Biol.* **2020**, *4*, 294.
(31) Aggarwal, N.; Garg, M.; Dwarakanathan, V.; Gautam, N.; Kumar, S. S.; Jadon, R. S.; Gupta, M.; Ray, A. Diagnostic accuracy of non-contact infrared thermometers and thermal scanners: a systematic review and meta-analysis. *J. Travel Med.* **2020**, *27*, taaa193.
(32) Walczak, K.; Sikorski, W. Non-contact high voltage measurement in the online partial discharge monitoring system. *Energies* **2021**, *14*, 5777.
(33) Zhang, X. M.; Jian, H.; Wang, Z. H.; Miao, Z. S.; Cheng, Y. B. Aging detection of silicon rubber composite insulator based on terahertz technology. *J. Guangxi Univ. Sci. Technol.* **2021**, *32*, 1−8.
(34) Shimaki, Y.; Senshu, H.; Sakatani, N.; Okada, T.; Fukuhara, T.; Tanaka, S.; Taguchi, M.; Arai, T.; Demura, H.; Ogawa, Y.; Suko, K.; Sekiguchi, T.; Kouyama, T.; Hasegawa, S.; Takita, J.; Matsunaga, T.; Imamura, T.; Wada, T.; Kitazato, K.; Hirata, N.; Hirata, N.; Noguchi, R.; Sugita, S.; Kikuchi, S.; Yamaguchi, T.; Ogawa, N.; Ono, G.; Mimasu, Y.; Yoshikawa, K.; Takahashi, T.; Takei, Y.; Fujii, A.; Takeuchi, H.; Yamamoto, Y.; Yamada, M.; Shirai, K.; Iijima, Y. I.; Ogawa, K.; Nakazawa, S.; Terui, F.; Saiki, T.; Yoshikawa, M.; Tsuda, Y.; Watanabe, S. I. Thermophysical properties of the surface of asteroid 162173 Ryugu: Infrared observations and thermal inertia mapping. *Icarus* **2020**, *348*, 113835.
(35) Doremalen, R. F. M. V.; Netten, J. J. V.; Baal, J. G. V.; Vollenbroek-Hutten, M. M. R.; Heijden, F. V. D. Infrared 3D thermography for inflammation detection in diabetic foot disease: a proof of concept. *J. Diabetes Sci. Technol* **2020**, *14*, 46−48.
(36) Thompsona, J. O.; Ramsey, M. S. Spatiotemporal variability of active lava surface radiative properties using ground-based multispectral thermal infrared data. *J. Volcanol Geoth. Res.* **2020**, *408*, 107077.
(37) Xu, L.; Gong, F. Q.; Liu, Z. X. Experiments on rockburst proneness of pre-heated granite at different temperatures: Insights from energy storage, dissipation and surplus. *J. Rock Mech. Geotech.* **2021**, *XX*, XX.
(38) Li, Z. H.; Lou, Q.; Wang, E. Y.; Liu, S. J.; Niu, Y. Study on acoustic−electric−heat effect of coal and rock failure processes under uniaxial compression. *J. Geophys. Eng.* **2018**, *15*, 71−80.
(39) Liu, X.; Liang, Z.; Zhang, Y.; Liang, P.; Tian, B. Experimental study on the monitoring of rockburst in tunnels under dry and saturated conditions using AE and infrared monitoring. *Tunnelling Underground Space Technol.* **2018**, *82*, 517−528.
(40) Chen, G. Q.; Zhang, Y.; Li, Y.; Pan, J. Y.; Jin, C. Y. Thermal-acoustic precursor information chain of rock failure under true triaxial loading. *Chin. J. Rock Mech. Eng.* **2021**, *40*, 1764−1776.
(41) Liu, C. Y.; Zhao, G. M.; Xu, W. S.; Meng, X. R.; Huang, S. J.; Zhou, J.; Wang, Y. K. Experimental investigation on failure process and spatio-temporal evolution of rockburst in granite with a prefabricated circular hole. *J. Cent. South Univ.* **2020**, *27*, 2930−2944.
(42) Huang, F. R.; Yan, S. X.; Wang, X. L.; Jiang, P. C.; Zhan, S. B. Experimental study on infrared radiation characteristics of gneiss under uniaxial compression. *J. Min. Strat. Control Eng.* **2021**, *3*, 96−103.
(43) Wang, B. X.; Wang, Y. B.; Fan, C. X.; Zhang, W. D. Energy distribution and evolution of frozen silty clay at subzero temperatures under compressive loading. *Transp. Geotech.* **2021**, 100656.
(44) Liu, Z. X.; Wang, W.; Luo, J. A.; Miu, G. H. Method of energy evolution of rock under uniaxial compression test. *J. China Coal Soc.* **2020**, *45*, 3131−3139.
(45) Song, D.; Wang, E.; Liu, J. Relationship between EMR and dissipated energy of coal rock mass during cyclic loading process. *Safety Sci.* **2012**, *50*, 751−760.
(46) Li, X.; Yang, Z.; Dai, S.; Qiu, B.; Xin, Y. Variation routine of surface infrared radiation temperature of composite coal rock in fracture under load. *China Saf. Sci. J.* **2017**, *27*, 110−115.
(47) Zhang, X. Y.; Zhou, B.; Li, H. Wind turbine blade defect depth detection based on three-dimensional heat conduction model. *Chin. J. Sci. Instrum.* **2021**, *42*, 174−182.
(48) Yang, Z.; Su, X. P.; Li, X. Stress-charge- temperature coupling model of composite coal-rock in deformation and fracture. *J. China Coal Soc.* **2019**, *44*, 2733−2740.

https://doi.org/10.1021/acsomega.1c07289
ACS Omega 2022, 7, 8060−8076

(49) Zhang, P.; He, T. H. A generalized thermoelastic problem with nonlocal effect and memory-dependent derivative. *Chin. J. Theor. Appl. Mech.* **2018**, *50*, 508−516.
(50) Xiong, Y. L.; Zhu, H. H.; Zhang, S.; Ye, G. L.; Zhang, F. A modified themo-elasto-viscoplastic constitutive model for soft rock considering the effect confining stress. *Chin. J. Rock Mech. Eng.* **2016**, *35*, 225−230.
(51) Chen, S.; Liu, L.; Liu, P.; Ma, J.; Chen, G. Theoretical and experimental study on relationship between stress-strain and temperature variation. *Sci. China, Ser. D: Earth Sci.* **2009**, *52*, 1825−1834.
(52) Perveiz, K. Thermoelastic relaxation and its effects on the compressibility of pore fluid and P wave velocities. *Ara J Geosci.* **2014**, *8*, 6157.
(53) Li, X.; Wang, X.; Yang, Z.; Li, H.; Li, Y.; Sun, W. Variation law of infrared radiation temperature of unloading fracture of composite coal-rock. *Geofluids* **2021**, *2021*, 7108408.
(54) Yang, Z.; Dai, S.; Li, X.; Qi, Q. J. Stress-electricity- thermal coupled of composite coal-rock in deformation and fracture under load. *J. China Coal Soc.* **2016**, *41*, 2764−2772.
(55) Ulhoa, S. C.; Santos, A. F.; Furtado, T. F.; Khanna, F. C. On gravitational casimir effect and stefan-boltzmann law at finite temperature. *Adv. High Energy Phys.* **2019**, 1.
(56) Wu, L.; Liu, S.; Wu, Y. Infrared imaging detection of water permeation on field large-scale rock relics. *IEEE T. Geosci. Remote* **2011**, *49*, 581−590.
(57) Gong, F.; Wang, Y.; Wang, Z.; Pan, J.; Luo, S. A new criterion of coal burst proneness based on the residual elastic energy index. *Int. J. Min. Sci. Technol.* **2021**, *31*, 553−563.
(58) Zhao, K.; Yu, X.; Zhou, Y.; Wang, Q.; Wang, J.; Hao, J. Energy evolution of brittle granite under different loading rates. *Int. J. Rock Mech. Min. Sci.* **2020**, 104392.
(59) Dong, F.; Zhu, T.; Huang, D. Experimental study on the energy characteristics of sandstone in direct shear test under a decreasing normal stress. *Ara J. Geosci.* **2021**, *14*, 1.
(60) Qi, H. Y. Research on underwater low frequency Electromagnetic wave propagation and internal wave electromagnetic scattering at sea surface. *Xidian Univ.* **2017**, *XX*, XX.
(61) Wan, G. X.; Wang, Q. S.; Li, X. B.; Cai, S. H. Propagation of electromagnetic radiation signal in metal ore. *China Tungsten Ind.* **2019**, *34*, 7−11.

https://doi.org/10.1021/acsomega.1c07289
ACS Omega 2022, 7, 8060−8076